Stable Potassium Isotopes ($^{41}K/^{39}K$) Track Transcellular and Paracellular Potassium Transport in Biological Systems

John A. Higgins[1*], Danielle Santiago Ramos[2], Stefania Gili[1], Cornelia Spetea[3,4], Scott Kanoski[5], Darren Ha[6], Alicia A. McDonough[6], Jang H. Youn[6]

[1]Department of Geosciences, Princeton University, Princeton, USA
[2]Department of Marine and Coastal Science, Rutgers University, New Brunswick, USA
[3]Department of Biological and Environmental Sciences, University of Gothenburg, Gothenburg, Sweden
[4]Department of Molecular Biology, Princeton University, Princeton, USA
[5]Department of Human and Evolutionary Biology, University of Southern California, Los Angeles, USA
[6]Department of Physiology and Neuroscience, University of Southern California Keck School of Medicine, Los Angeles, USA

*corresponding author: email: jahiggin@princeton.edu; phone 617-852-9931

Abstract: As the most abundant cation in archaeal, bacterial, and eukaryotic cells, potassium (K^+) is an essential element for life. While much is known about the machinery of transcellular and paracellular K transport – channels, pumps, co-transporters, and tight-junction proteins - many quantitative aspects of K homeostasis in biological systems remain poorly constrained. Here we present measurements of the stable isotope ratios of potassium ($^{41}K/^{39}K$) in three biological systems (algae, fish, and mammals). When considered in the context of our current understanding of potential mechanisms of K isotope fractionation and K^+ transport in these biological systems, our results provide evidence that the fractionation of K isotopes depends on transport pathway and transmembrane transport machinery. Specifically, we find that passive transport of K^+ down its electrochemical potential through channels and pores in tight-junctions at favors ^{39}K, a result which we attribute to a kinetic isotope effect associated with dehydration and/or size selectivity at the channel/pore entrance. In contrast, we find that transport of K^+ against its electrochemical gradient via pumps and co-transporters is associated with less/no isotopic fractionation, a result that we attribute to small equilibrium isotope effects that are expressed in pumps/co-transporters due to their slower turnover rate and the relatively long residence time of K^+ in the ion pocket. These results indicate that stable K isotopes may be able to provide quantitative constraints on transporter-specific K^+ fluxes (e.g. the fraction of K efflux from a tissue by channels vs. co-transporters) and how these fluxes change under different physiological states. In addition, precise determination of K isotope effects associated with K^+ transport through channels, pumps, and co-transporters may provide unique constraints on the mechanisms of K transport that could be tested with steered molecular dynamic simulations.

Keywords: potassium, homeostasis, stable isotope, physiology

1. Introduction

Archaeal, bacterial, and eukaryotic cells all concentrate potassium (K^+). In fact, the ubiquity of elevated intracellular K^+ has been hypothesized to provide insight into the environments (high K/Na ratios) where the first cells emerged (Mulkidjanian et al., 2012). In bacteria, intracellular K^+ is at >100 mM by the active pumping of K^+ from extracellular fluid (ECF) into the intracellular fluid (ICF) by transporters that use ATP or the proton motive force (Stautz et al., 2021). In eukaryotic cells, intracellular K^+ is maintained at similarly elevated levels by the active pumping of K^+ by plasma membrane Na,K-ATP_{ase}, an energetically intensive process which can account for ~20% of basal metabolism in mammals (Rolfe and Brown, 1997). In all cells, the active transport of K^+ into the cell establishes a steep transmembrane gradient that is a key determinant of membrane potential and a source of energy to drive action potentials, control muscle contractility,

maintain cell turgor, contribute to pH homeostasis, and power ion transporters (Stautz et al., 2021; Youn and McDonough, 2009).

The regulation of K^+ at both the cellular and organismal level, K^+ homeostasis, is ultimately accomplished at the molecular level by transcellular and paracellular transporters (including ion pumps, channels, co-transporters) that move K^+ across membranes and between cells (Agarwal et al., 1994; Furukawa et al., 2012; Gierth and Mäser, 2007; Youn and McDonough, 2009). Although life has evolved a diversity of molecular machines capable of K^+ transport across cell membranes, certain aspects of cellular K^+ transport are conserved across the major domains. For example, all known K^+ channels are members of a single protein family whose amino acid sequence contains a highly conserved segment (the K^+ channel signature sequence (MacKinnon, 2003)). The shared molecular machinery of K^+ transport in biological systems reflects the fundamental role of the electrochemical potential generated by biologically maintained gradients of K^+ across cell membranes. K^+ pumps establish and maintain concentration gradients across cell membranes by moving K^+ (from ECF-ICF) and Na or H (from ICF to ECF) "uphill" against their electrochemical potentials coupled to and driven by the hydrolysis of ATP. K^+ co-transporters couple uphill K^+ transport to "downhill" transport of another ion (e.g., Na^+ or Cl^-). Finally, K^+ channels and the pores in tight-junction proteins provide an energetically favorable pathway for rapid, yet highly selective, transport of K^+ down its electrochemical potential.

While the identity and structure of the molecular machines that maintain K^+ homeostasis in biological systems are well-known, many quantitative aspects of K^+ homeostasis and the specific mechanisms of K^+ transport by pumps, channels, co-transporters, and through tight-junction proteins are unconstrained or debated. For example, structural, functional and computational studies of K^+ channels produce conflicting results as to whether the molecular mechanism of K^+ permeation is water mediated or occurs by direct knock-on of cations (Mironenko et al., 2021). In addition, while studies of gene expression in cells and tissues can be used to identify which K transporters are active, quantitative constraints on the fluxes of K^+ through the different types of transporters *in vivo* are non-existent.

In natural systems potassium is made up of two stable (potassium-39 and potassium-41) and one radioactive (potassium-40) isotope. The two stable isotopes of K, ^{39}K and ^{41}K, constitute 93.258% and 6.730% of the total, respectively, resulting in a ratio of $^{41}K/^{39}K$ in nature of ~0.07217. Recent advances in inductively coupled plasma mass spectrometry (ICP-MS) now permit the precise quantification of deviations from the terrestrial ratio resulting from the biogeochemical cycling of potassium in nature with a precision of 1 part in 10,000 (Morgan et al., 2018; Wang and Jacobsen, 2016). Here we apply this analytical tool to study K^+ homeostasis in three biological systems – aquatic green alga *Chlamydomonas reinhardtii* (*C. reinhardtii*), a suite of marine fish that include

species that can tolerate a wide range in salinities (euryhaline) as well as those that have a restricted salinity range (stenohaline), and the terrestrial mammal *Rattus norvegicus* (*R. norvegicus*). The results in each system are interpreted as reflecting K^+ homeostasis under normal (optimal) growth conditions. The data are presented using standard delta notation in parts per thousand (‰).

$$\delta^{41/39}\mathrm{K} = \left({\mathrm{R}_{\mathrm{sample}}^{^{41}\mathrm{K}/^{39}\mathrm{K}}} \Big/ {\mathrm{R}_{\mathrm{standard}}^{^{41}\mathrm{K}/^{39}\mathrm{K}}} - 1 \right) \cdot 10^3$$

where $\mathrm{R}_{\mathrm{sample}}^{^{41}\mathrm{K}/^{39}\mathrm{K}}$ is the ratio of $^{41}K/^{39}K$ in a sample and $\mathrm{R}_{\mathrm{standard}}^{^{41}\mathrm{K}/^{39}\mathrm{K}}$ is the $^{41}K/^{39}K$ of the standard). For plants the standard is the $^{41}K/^{39}K$ of the growth medium, whereas for marine teleosts it is the $^{41}K/^{39}K$ of seawater. For *R. norvegicus*, we report the data in one of two ways. To explore total body K^+ homeostasis we report the $^{41}K/^{39}K$ of K excretory losses normalized to the $^{41}K/^{39}K$ of the diet whereas to examine the partitioning of K isotopes between extracellular and intracellular compartments we report the $^{41}K/^{39}K$ of tissues relative to the $^{41}K/^{39}K$ of blood plasma or cerebrospinal fluid (CSF). K isotope fractionation factors are calculated as ratios of isotope ratios (e.g. $\alpha_{medium/cell} = [^{41}K/^{39}K_{medium}] / [^{41}K/^{39}K_{cell}]$) and reported as ε values (in ‰) where $\varepsilon_{medium/cell} = \alpha_{medium/cell} - 1$.

2. **Materials and Methods**

C. reinhardtii cultures: The CMJ030 wild type strain was obtained from the Chlamydomonas culture collection www.chlamycollection.org). Tris Phosphate (TP) medium was prepared according to: Gorman, D.S., and R.P. Levine (1965) Proc. Natl. Acad. Sci. USA 54, 1665-1669. The culture at an initial density of 0.5 $x10^5$ cells mL^{-1} was grown in TP under continuous illumination (100 µmol photons m^{-2} s^{-1}) and shaking for four days. Samples (in triplicate) containing 2 $x10^7$ cells (~800 mg) were harvested and washed twice in 5 mM HEPES and 2 mM EDTA before collection and air-drying of the cell pellet. Pelletized cells (~30mg) were digested in screw-capped teflon vials on a hot plate at elevated temperatures (~75 °C) using a 5:2 mixture of HNO_3 (68-70 vol.%) and H_2O_2 (30 vol.%).

Euryhaline and stenohaline marine teleosts: Samples of teleost muscle tissue were sourced from fish markets (Nassau Seafood and Trader Joe's in Princeton, NJ and the Fulton Fish Market in Brooklyn, NY) and research cruises (NOAA NEFSC Bottom Trawl Survey, Fall 2015 and Spring 2015). All teleosts were caught in seawater which has a uniform $\delta^{41}K$ value of +0.12‰ relative to SRM3141a (Ramos et al., 2020). Samples of white dorsal muscle (100 to 3000 mg) were digested on a hot plate at elevated temperatures (~75 °C) or in a high-pressure microwave system (MARS 6) using HNO_3 (68-70 vol.%) H_2O_2 (30 vol.%) in a ratio of 5:2. Major/minor element analyses for digested samples were carried out at Princeton University using a quadrupole inductively

133 coupled plasma mass spectrometer (Thermo Scientific iCap Q). Concentrations and
134 elemental ratios were determined using externally calibrated standards and average
135 uncertainties (element/element) are ~10%.

136 *R. norvegicus experiments:* All rat experiments were approved by the Institutional Animal
137 Care and Use Committees of the University of Southern California. Two series were
138 conducted. Series #1: Male Wistar rats (n=3, 250-275g body weight, Envigo,
139 Indianapolis, IN) were housed in a climate controlled (22-24°C) environment with a 12
140 hr: 12hr light/dark cycle, and fed casein based normal K^+ diet TD.08267 (Envigo,
141 Indianapolis, IN) and water ad libitum for 11 days. At day 8, rats were placed overnight
142 into metabolic cages (Techniplast, Buguggiate, Italy) with food and water ad libitum for
143 16-hour collection of urine and feces. On termination day (1:30-3:30PM), rats were
144 anesthetized with an intramuscular (IM) injection of ketamine (80 mg/kg, Phoenix
145 Pharmaceuticals, St. Joseph, MO) and xylazine (8 mg/kg, Lloyd Laboratories,
146 Shenandoah, IA) in a 1:1 ratio. Through a midline incision, the liver, kidneys, heart, fat
147 pads, and stomach (flushed of contents) were removed; blood was collected via cardiac
148 puncture, spun down to separate plasma from RBCs. Then gastrocnemius, soleus, TA,
149 and EDL skeletal muscles were dissected. All tissues were washed in ice-cold TBS to
150 remove excess blood, weighed and snap frozen in liquid nitrogen. Series #2: Male
151 Sprague Dawley rats (n=4, 250-300g, Envigo, Indianapolis, IN) were housed in a climate
152 controlled (22-24°C) environment with a 12 hr: 12hr light/dark cycle and fed grain-based
153 vivarium chow (LabDiet 5001, labdiet.com). CSF extraction procedures are as reported
154 previously (Noble et al., 2018). In brief, Rats were deeply anesthetized using a cocktail
155 of ketamine 90mg/kg, xylazine, 2.8 mg/kg, and acepromazine 0.72 mg/kg by
156 intramuscular injection. A needle was lowered to below the caudal end of the occipital
157 skull and the syringe plunger pulled back slowly, allowing the clear CSF to flow into the
158 syringe. After extracting ~100-200 μl of CSF, the needle was raised quickly (to prevent
159 suction of blood while coming out of the cisterna magna) and the CSF dispensed into a
160 microfuge tube and immediately frozen in dry ice and then stored at -80 °C until time of
161 analysis. Following CSF extraction and decapitation, whole brains with 10-15mm spinal
162 cord extension were rapidly removed and immediately flash frozen and stored in -80°C
163 until dissection into spinal cord, cerebrum, and cerebellum for subsequent digestion and
164 K isotopic analysis.

165 *Ion chromatography and isotope ratio mass-spectrometry:* K was purified for isotopic
166 analyses using an automated high-pressure ion chromatography (IC) system. The IC
167 methods utilized here followed those previously described in (Morgan et al., 2018;
168 Ramos et al., 2018). The accuracy of our chromatographic methods was verified by
169 purifying and analyzing external standards (SRM3141a and SRM70b) alongside
170 unknown samples. Purified aliquots of K were analyzed in 2% HNO_3 for their isotopic
171 compositions on a Thermo Scientific Neptune Plus multi-collector inductively coupled
172 plasma mass spectrometer (MC-ICP-MS) at Princeton University, using previously
173 published methods (Morgan et al., 2018; Ramos et al., 2020). The external
174 reproducibility of our protocols (chromatography and mass spectrometry) was
175 determined through replicate measurements of international standards. Measured

values of SRM70b, reported relative to SRM3141 ($\delta^{41}K_{SRM3141}$) are -0.57 ± 0.17‰ (2σ; N = 59), indistinguishable from published values (Ramos et al., 2018; Ramos et al., 2020; Wang and Jacobsen, 2016). For samples analyzed once (chromatography and mass spectrometry), reported errors are the 2σ uncertainties of the external standard. In cases where samples were analyzed multiple times, reported errors in are twice the standard error of the mean (2 S.E. or 95% confidence).

3. Results

Results for the freshwater algae *C. reinhardtii* are shown in Figure 1. Measured $\delta^{41}K$ values of the whole cells are 1.2±0.07‰ lower than the $\delta^{41}K$ value of the growth medium (0‰ by definition) (95% confidence; $P = 4.5x10^{-5}$).

Results for *R. norvegicus* are shown in Figures 2-4. Measured $\delta^{41}K$ values of both urine and feces, normalized to the $\delta^{41}K$ value of the rat diet ($\delta^{41}K_{diet}$), indicate preferential net uptake of ^{39}K relative to ^{41}K across the gut epithelium leading to a positive $\delta^{41}K_{diet}$ value in feces (+0.19±0.09‰, 95% confidence; $P = 0.037$; Fig. 2) and slightly negative $\delta^{41}K_{diet}$ value in urine (-0.09±0.10‰, 95% confidence; $P = 0.1895$).

Measurements of K isotopes of various tissues in *R. norvegicus* (except brain tissues) are normalized to the $\delta^{41}K$ value of the blood plasma ($\delta^{41}K_{plasma}$), as this represents the extracellular K concentration bathing the tissues. For brain tissues, measured $\delta^{41}K$ values are normalized to CSF ($\delta^{41}K_{CSF}$) for the same reason. The overall range in $\delta^{41}K_{plasma}$ values between different tissues and fluids is ~1‰ (Figs. 3,4); $\delta^{41}K$ values of the following tissues are elevated in ^{41}K relative to blood plasma (positive $\delta^{41}K_{plasma}$ values): red blood cells (+0.40±0.08‰, $P = 0.005$), heart (+0.55±0.15‰, $P = 0.0047$), liver (+0.30±0.05‰, $P = 0.01$), and soleus muscle (+0.17±0.03‰, $P = 0.05$). Similarly, brain tissues are elevated in ^{41}K relative to CSF (positive $\delta^{41}K_{CSF}$ values): cerebrum (+0.34±0.15‰, $P = 0.012$), spinal cord (+0.30±0.17‰, $P = 0.026$), and cerebellum (+0.21±0.11‰, $P = 0.037$). In contrast, urine (-0.50±0.10‰, $P = 0.0019$) and CSF (-0.59±0.12‰, $P = 6.2x10^{-5}$) are characterized by negative $\delta^{41}K_{plasma}$ values. In another category are tissues with $\delta^{41}K_{plasma}$ values that are statistically indistinguishable from zero including: kidneys (+0.07±0.07‰, $P = 0.31$), adipose tissue (+0.01±0.08‰, $P = 0.92$), extensor digitorum longus (EDL, +0.17±0.11‰, $P = 0.099$) gastrocnemius (+0.01±0.15‰, $P = 0.92$), and tibialis anterior (TA, +0.09±0.1‰, $P = 0.30$).

Results for white muscle tissue from a suite of stenohaline and euryhaline marine fish, reported relative to the $^{41}K/^{39}K$ of seawater ($\delta^{41}K_{seawater}$ = 0‰) are shown in Figure 5a. The total range in muscle $\delta^{41}K$ values is ~2‰ (+1‰ to -1‰). Stenohaline species including *Gadus morhua* (Atlantic Cod), *Peprilus striacanthus* (Butterfish), Xiphias gladius (Swordfish), *Pseudopleuronectes americanus* (Winter Flounder), and

Hippoglossus stenolepis (Pacific Halibut) are characterized by $\delta^{41}K_{seawater}$ values that are uniformly negative whereas the euryhaline species *Oncorhynchus kisutch* (Coho Salmon), *Oncorhynchus tshawytscha* (King Salmon), and *Oncorhynchus nerka* (Sockeye Salmon) are characterized by $\delta^{41}K_{seawater}$ values that are close to zero or positive. When species are grouped by salinity tolerance, average measured $\delta^{41}K_{seawater}$ values of the two groups are -0.58±0.09‰, and 0.29±0.18‰ for stenohaline and euryhaline species, respectively (95% confidence; $P = 1.4x10^{-10}$).

4. **Discussion**

The shared machinery of K^+ transport across the domains of life suggests that the variability in K isotopes observed in biological systems can be reduced to a consideration of 1) how different classes of K^+ transporters - tight junctions, channels, pumps, and co-transporters - discriminate between ^{39}K and ^{41}K and 2) how these transporters are assembled into a homeostatic system. The extent to which K^+ transporters fractionate K isotopes will, in turn, depend on the mechanics and selectivity of the transporter and whether the binding of dissolved K^+ to transporter is the rate-limiting step. In particular, K^+ channels and pores in tight-junction proteins are both associated with selective and rapid (near the limit of diffusion) transport of K^+ where the rate-limiting step is the binding of dissolved K^+ to the transporter/selectivity filter. These conditions favor kinetic isotope effects which may arise from either partial or full desolvation of K^+ as it binds to the selectivity filter (Berneche and Roux, 2003; Hofmann et al., 2012; Kopec et al., 2018; Yu et al., 2010), differences in ionic radius of ^{39}K and ^{41}K (size selectivity (Christensen et al., 2018)), or some combination of the two. Critically, the magnitude of the kinetic isotope effects associated with both desolvation and/or size selectivity appear to be large, with estimates from laboratory experiments and molecular dynamic simulations ranging from ~1 to 2.7‰ (Hofmann et al., 2012).

In contrast to channels and pores in tight-junction proteins, transport of K^+ by pumps and co-transporters is relatively slow (per unit transporter, (Roux, 2017)), requires the simultaneous binding of multiple ions (e.g. 2 K^+ ions in the case of Na,K-ATPase), and is associated with mechanisms of self-correction that prevent the pump cycle from proceeding if incorrect ions bind to the ion pocket (Rui et al., 2016). As a result, although the binding of K^+ to the active site of a pump or cotransporter may also involve desolvation, it is not the rate-limiting step in K^+ transport. In this case, the isotopic composition of K^+ that is transported by pumps and co-transporters may reflect isotopic equilibration between K^+ in the ion pocket and the fluid due to the longer residence time of K^+ in the ion pocket prior to occlusion. As equilibrium K isotope effects tend to be small (Li et al., 2017; Ramos et al., 2018; Zeng et al., 2019), we hypothesize that K^+ transport by pumps and co-transporters will be associated with less isotopic fractionation.

In the following sections we show how our results for the three studied biological systems (algae, fish, mammals) can be interpreted within a single framework where K^+ transport by channels and pores in tight-junction proteins are associated with large (kinetic) K isotope effects whereas K^+ transport by pumps and/or co-transporters is associated with smaller (equilibrium) K isotope effects. In simple biological systems (e.g. single celled alga) linking K isotope fractionation to the machinery of K^+ transport is relatively straightforward due to the small number of pathways involved and the unidirectional nature of K^+ transport. In more complex biological systems (e.g. higher plants, fish, and mammals) discerning transporter-specific fractionation of K isotopes is more difficult for at least two reasons. First, our understanding of K homeostasis at both the tissue and organism level is incomplete. Second, our measured K isotopic differences (e.g. between plasma/CSF/seawater and tissue) only provide information on net K isotope fractionation associated with bi-directional K^+ transport at steady-state. In spite of these limitations, our results support a framework for K isotope fractionation in biological systems that can provide new quantitative insights into the mechanisms of K^+ transport and the dynamics of K homeostasis.

4.1 Algae. As an essential macronutrient in all plants and the most abundant cation in the cytoplasm, K^+ contributes to electrical neutralization of anionic groups, membrane potential and osmoregulation, photosynthesis, and the movements of stomata (Gierth and Mäser, 2007; Marchand et al., 2020). It is well-established that K^+ channels play prominent roles in K^+ uptake (Lebaudy et al., 2007). For example, under normal growth conditions ($[K^+]_{ext}$ ~1 mM; (Epstein et al., 1963; Kochian and Lucas, 1982; Malhotra and Glass, 1995)) K^+ uptake in plants is dominated by transport via inward-rectifying K^+ channels electrically balanced by the ATP-driven efflux of H^+ (Britto and Kronzucker, 2008; Hirsch et al., 1998). Considered in this context our results for whole cells of *C. reinhardtii* can be interpreted as reflecting K isotope fractionation associated with uptake via K^+ channels ($\varepsilon_{\mathrm{in}} = \delta^{41}\mathrm{K}_{\mathrm{medium}} - \delta^{41}\mathrm{K}_{\mathrm{cell}}$ = ~1.2‰; Figure 1). Although we cannot guarantee that K uptake occurs exclusively via K^+ channels, this result represents our best estimate of a transporter-specific K isotope effect ($\varepsilon_{\mathrm{ch}}$). The magnitude of this effect is smaller than modeled estimates of the kinetic isotope effect associated with ion desolvation (Hofmann et al., 2012) and of the same order as hypothesized kinetic isotope effects associated with size-selectivity (Christensen et al., 2018).

4.2 Higher Plants. Our result for K isotope fractionation associated with K^+ uptake in *C. reinhardtii* is similar in sign, though somewhat larger in magnitude, than the K isotope effect associated with K^+ uptake estimated by Christensen et al. (2018) in experiments involving higher plants. Those authors analyzed the δ^{41}K values of the roots, stems, and leaves of *Triticum aestivum* (wheat), *Glycine max* (soy) and *Oryza sativa* (rice) grown under hydroponic conditions and observed systematic differences in the δ^{41}K value of the different reservoirs. In particular, roots, stems, and leaves exhibited increasingly

negative $\delta^{41}K$ values (Figure S1). Compared to the freshwater alga *C. reinhardtii*, quantifying transport-specific K isotope effects in higher plants is more complex as the $\delta^{41}K$ value of each individual compartment (root, stem, leaf) reflects a balance between isotopic sources and sinks (e.g. the $\delta^{41}K$ value of the root will depend on K isotope effects associated with both net K^+ uptake as well as translocation and recycling). Using a model of K isotope mass balance that includes assumptions regarding plant growth and the partitioning of K^+ fluxes between translocation and recycling, Christensen et al. (2018) estimated large K isotope effects for uptake (ε_{in} ~0.7 to 1.0‰) and translocation from root to stem (~0.6‰), but smaller isotopic effects (0 to 0.2‰) for translocation of K^+ from stem to leaf and recycling of K^+ from leaf to root. Interestingly, in addition to their important role in K^+ uptake, K^+ channels have also been shown to be involved in translocation (root to stem; (Gaymard et al., 1998)) providing a potential explanation for the relatively large K isotope effect observed by Christensen et al. (2018) for this process. In contrast, translocation and recycling of K^+ from leaf to root, a process that also involves K^+ channels (Lacombe et al., 2000; Pilot et al., 2001), does not appear to result in significant fractionation of K isotopes. This could be due to the increased importance of other types of K^+ transporters in this process, a reduction in the expression of K isotope fractionation by channels due to rapid internal recycling of K^+ between stem and leaf (compared to K^+ transport from root to stem), or some combination of the two.

4.3 Terrestrial Mammals. K^+ homeostasis in terrestrial mammals reflects the balance between K^+ gained from diet and K^+ lost in urine and feces (Figure 2, Figure 3a). This balance is largely achieved by the kidneys and colon, which possess a remarkable ability to sense a change in K^+ in the diet and then appropriately adjust K^+ loss in response. ECF (which includes blood plasma), the reservoir through which internal K^+ is exchanged, represents only 2% of total body K^+. Though small, this reservoir is tightly regulated to maintain membrane potential as indicated by the narrow range of normal ECF [K^+] (~ 3.5 – 5 mEq/L,)(Boron, 2005; McDonough and Youn, 2017). Of the remaining 98% of total body K^+, 75% resides in muscle tissues ([K^+] ~ 130 mEq/L) and 23% in non-muscle tissues. Some tissues, particularly skeletal muscle, are critical to K^+ homeostasis by providing a buffering reservoir of K^+ that can take up K^+ after a meal and altruistically donate K^+ to ECF to maintain blood plasma levels during fasting. Cerebrospinal fluid (CSF), the body fluid that surrounds the brain and spinal cord of all vertebrates, merits special mention as its K^+ content is even more tightly regulated than ECF (Bradbury and Davson, 1965).

4.3.1. External K isotope mass balance in terrestrial mammals. Roughly ~80-90% of K in the diet is lost in urine with the remainder lost in feces (Agarwal et al., 1994). Uptake of K^+ across gut endothelial cells occurs largely paracellularly through pores in tight-junction proteins like caudin-15 (Garcia-Hernandez et al., 2017) as a result of the

329 transmucosal electrical potential difference (Barnaby and Edmonds, 1969). However,
330 transcellular K^+ uptake (via pumps) and secretion (via channels) has also been shown to
331 occur in gut epithelial cells (Foster et al., 1984). As a result, K isotope fractionation
332 associated with net K uptake in the gut will reflect the flux-weighted average of the K
333 isotope fractionation associated with both transcellular and paracellular K^+ transport. The
334 observation that feces is characterized by a positive $\delta^{41}K_{diet}$ value and urine with a
335 slightly negative $\delta^{41}K_{diet}$ value (Figure 2) indicates that the net K isotope effect
336 associated with K uptake under these conditions (ε_{gut}) is ~0.2‰ (Figure 3b). Relative to
337 the diet, internal tissues of *R. norvegicus* exhibit a 1‰ range from -0.04‰ for the
338 cerebellum to +1.05‰ for the heart (Figure 2). Assuming an internal K^+ distribution that
339 is 75/15/10 muscle/adipose/other tissues, a reasonable average whole-body $\delta^{41}K_{diet}$
340 value of *R. norvegicus* is ~+0.5‰. As net uptake of K^+ in the gut prefers ^{39}K, the elevated
341 average whole-body $\delta^{41}K_{diet}$ of *R. norvegicus* requires that there be even greater K
342 isotope fractionation (favoring ^{39}K) associated with K^+ loss in the urine (see below).

343 *4.3.2 Internal K isotope mass balance in terrestrial mammals***.** As shown in Figures 3a
344 and 4, measured $\delta^{41}K$ values of the 16 different tissues and fluids analyzed in *R.*
345 *norvegicus* fall into 3 distinct categories relative to ECF ($\delta^{41}K_{plasma}$ or $\delta^{41}K_{CSF}$): those with
346 positive $\delta^{41}K_{plasma/CSF}$ values (red blood cells, heart, liver, soleus muscle and brain
347 tissues), those with $\delta^{41}K_{plasma/CSF}$ values that are close to 0 (stomach, adipose tissue,
348 kidney, gastrocnemius, EDL and TA muscles), and those with negative $\delta^{41}K_{plasma/CSF}$
349 values (urine and CSF).

350 The timescale for K^+ turnover in the studied tissue/cell/fluid reservoirs is rapid
351 (e.g. 0.9-10%/min; (Jones et al., 1977; Terner et al., 1950)). As a result, for all measured
352 tissues/cells, the $\delta^{41}K$ values in Figure 3a can be interpreted as reflecting steady-state K
353 isotope mass balance between the tissue/cell/fluid and the relevant fluid (blood
354 plasma/ECF or CSF). At isotopic steady-state, the $\delta^{41}K$ value of K^+ entering the reservoir
355 must equal to $\delta^{41}K$ value of K^+ leaving the reservoir. As a result, reservoirs with
356 $\delta^{41}K_{plasma/CSF}$ values that differ from 0‰ require that net K^+ transport in one direction
357 results in greater fractionation of K isotopes than net K^+ transport in the opposite
358 direction. For example, reservoirs with positive $\delta^{41}K_{plasma}$ values including red blood cells,
359 heart, liver, and soleus require that K^+ transport from ICF to plasma or ECF is associated
360 with a larger K isotope effect than K^+ transport from ECF to ICF. The same relationship
361 is observed between brain tissues and CSF (Figure 4). Similarly, reservoirs with
362 $\delta^{41}K_{plasma}$ values that are close to 0‰ require that net K^+ transport in both directions does
363 not fractionate K isotopes, i.e., the isotope effects must be of equal magnitude and sign
364 and cancel. These include kidney, adipose tissue, stomach, and gastrocnemius and TA
365 muscles. Finally, the negative $\delta^{41}K_{plasma}$ values for CSF requires that net K^+ transport
366 from ECF to CSF through the choroid plexus and blood brain barrier (BBB) is

characterized by a K isotope effect that is ~0.6‰ greater than the K isotope effect associated K^+ transport from CSF to ECF (Figure 4).

Quantitatively linking the observed isotopic differences between ECF and ICF of various tissues/cells to the machinery of K^+ homeostasis in complex biological systems is complicated by both an incomplete understanding of the machinery involved and limitations of steady-state isotopic mass balance. In particular, although much is known about the identity and molecular structure of the machinery that maintains K^+ homeostasis, quantitative information on how each transporter contributes to the gross fluxes of K^+ between ICF and ECF at the resting membrane potential is lacking. For example, in red blood cells, probably the best understood with regard to the machinery of K^+ homeostasis due to the fundamental role it plays in the regulation of cell volume and longevity (Tosteson and Hoffman, 1960), elevated intercellular K^+ is believed to be maintained by a 'pump-leak' mechanism where the pump is Na,K-ATP_{ase} and the leak is K^+ channels (Gardos, 1958). However, red blood cells also show activity for co-transporters such as NKCC (Duhm, 1987; Sachs, 1971) and KCC (Franco et al., 2013), as well as inward-rectifying K^+ channels (Hibino et al., 2010), and exactly how much K^+ is transported by which transporter at the resting membrane potential is not well known.

In order to evaluate whether or not differences in measured $\delta^{41}K_{plasma}$ values reflect quantitative differences in K^+ fluxes through various transporters, we developed a generic model of K homeostasis (Figure 3b) that assumes 1) the tissue/cell is at the resting membrane potential and K is at isotopic steady-state between ECF and ICF, 2) all channels fractionate K isotopes identically ($\varepsilon_{\mathrm{ch}}$), 3) all pumps and co-transporters fractionate K isotopes identically ($\varepsilon_{\mathrm{p/co}}$), and 4) pumps, co-transporters, and channels may transport K^+ in either direction ($\mathrm{F}^{in}_{\mathrm{p/co}}$, $\mathrm{F}^{out}_{\mathrm{p/co}}$, $\mathrm{F}^{in}_{\mathrm{ch}}$, and $\mathrm{F}^{out}_{\mathrm{ch}}$):

$$\mathrm{F}^{in}_{\mathrm{p/co}} + \mathrm{F}^{in}_{\mathrm{ch}} = \mathrm{F}^{out}_{\mathrm{p/co}} + \mathrm{F}^{out}_{\mathrm{ch}} \quad (1)$$

$$(\delta^{41}K_{ECF} - \varepsilon_{\mathrm{p/co}}) \cdot \mathrm{F}^{in}_{\mathrm{p/co}} + (\delta^{41}K_{ECF} - \varepsilon_{\mathrm{ch}}) \cdot \mathrm{F}^{in}_{\mathrm{ch}} = (\delta^{41}K_{ICF} - \varepsilon_{\mathrm{p/co}}) \cdot \mathrm{F}^{out}_{\mathrm{p/co}} + (\delta^{41}K_{ICF} - \varepsilon_{\mathrm{p/co}}) \cdot \mathrm{F}^{out}_{\mathrm{ch}} \quad (2)$$

where $\varepsilon_{\mathrm{ch}}$, and $\varepsilon_{\mathrm{p/co}}$ are the K isotope fractionation factors associated with channels and pumps/co-transporters, respectively. Solving for the $\Delta\delta^{41}K_{plasma}$ value of the ICF ($\delta^{41}K_{ICF}$ - $\delta^{41}K_{ECF}$) yields:

$$\delta^{41}K_{plasma}\ (‰) = \Delta \mathrm{f}_{\mathrm{ch}} \cdot (\varepsilon_{\mathrm{ch}} - \varepsilon_{\mathrm{p/co}}) \quad (3)$$

where $\Delta \mathrm{f}_{\mathrm{ch}} = \mathrm{f}^{out}_{\mathrm{ch}} - \mathrm{f}^{in}_{\mathrm{ch}}$, $\mathrm{f}^{in/out}_{\mathrm{ch}} = \mathrm{F}^{in/out}_{\mathrm{ch}} / (\mathrm{F}^{in/out}_{\mathrm{ch}} + \mathrm{F}^{in/out}_{\mathrm{p/co}})$. Assuming, based on our results for *C. reinhardtii*, that $\varepsilon_{\mathrm{ch}} \sim 1.2‰$ and speculating, based on analogues with equilibrium K isotope effects associated with mineral precipitation in aqueous systems (Li et al., 2017; Ramos et al., 2018; Zeng et al., 2019), that $\varepsilon_{\mathrm{p/co}} \sim 0‰$, reduces eqn (1) to:

$$\delta^{41}K_{plasma}\ (‰) = 1.2 \cdot \Delta f_{ch} \quad (4)$$

As $f_{ch}^{in/out}$ represent fractions of a flux, the value of Δf_{ch} is bounded at ±1; +1 representing a perfect 'pump-leak' mechanism, -1 representing a perfect 'leak-pump' mechanism, and 0 consistent with either a 'pump-pump' or 'leak-leak' mechanism. Accordingly, $\Delta\delta^{41}K_{plasma}$ values are bounded at ±1.2‰, with +1.2‰ representing a perfect 'pump-leak' mechanism, -1.2‰ representing a perfect 'leak-pump' mechanism, and 0‰ representing either a 'pump-pump' or 'leak-leak' mechanism. The observation that the $\Delta\delta^{41}K_{plasma}$ values of all internal reservoirs are ≥ 0 suggests that $\Delta f_{ch} \geq 0$, a result that is qualitatively consistent with the idea of elevated intercellular K^+ being maintained by a 'pump-leak' mechanism. However, $\delta^{41}K_{plasma}$ values of the analyzed reservoirs also exhibit a considerable range, from ~0‰ for many skeletal muscles to +0.55‰ for the heart. In the context of eqn. (1), these differences can be explained by an increase in the relative importance of K^+ loss via channels. Skeletal muscles appear to maintain K homeostasis by something closer to a 'pump-pump' or 'leak-leak' mechanism whereas red blood cells, the liver and the heart approach ~50% of a perfect 'pump-leak' mechanism.

Two lines of evidence provide additional independent support for our interpretation of $\delta^{41}K_{plasma}$ values as quantitative indicators of the relative importance of K^+ loss from ICF via channels (eqn. (3)). First, measured $\delta^{41}K_{plasma}$ values are correlated with the activity of $NaKATP_{ase}$ (umol P/h per g tissue) in tissues where this activity is related to the maintenance of intercellular [K^+]. In particular, $NaKATP_{ase}$ activity increases from 91±15 in skeletal muscles, to 253±8 in the liver, and 351±23 in the heart (Gick et al., 1993). All else held constant, this increase in $NaKATP_{ase}$ activity (K^+ sources to the ICF via pumps) will lower f_{ch}^{in} and increase Δf_{ch}, in agreement with observations. Second, measured $\delta^{41}K_{plasma}$ values also correlate with intercellular [K^+] (Figure 4c). Because intercellular [K^+] reflects the balance between K^+ the sources and sinks to the ICF, one possible explanation for lower intercellular [K^+] is a reduction in K^+ supply and/or an increase in K^+ loss. As K^+ supply from $NaKATP_{ase}$ increases (see above), the most likely alternative explanations are a decline in K^+ supply from inward rectifying K^+ channels and/or an increase in K^+ loss via outward rectifying K^+ channels. Both of these processes increase Δf_{ch} and result in higher $\delta^{41}K_{plasma}$ values, again in agreement with observations.

4.3.2.1 Urine. Unlike the internal K^+ reservoirs discussed above, all of which are interpreted as independent homeostatic systems at isotopic steady-state with respect to ECF (plasma), the loss of K^+ through the urine represents the end product of a series of steps each of which may contribute to the observed net K isotope fractionation (e.g. Figure 3b; $\varepsilon_{kidney} \sim 0.50‰$). These are 1) glomerular filtration, 2) reabsorption along the proximal tubule and the thick ascending limb of the loop of Henle, and 3) secretion and

reabsorption by principal and intercalated collecting duct cells. Although a detailed description of the potential K isotope effects associated with each step is beyond the scope of this manuscript, a brief description follows. Glomerular filtration is not expected to fractionate K isotopes as the slit diaphragms freely filter ions and small molecules. A large fraction (~85%) of the filtered K^+ is subsequently reabsorbed via both paracellular and transcellular routes in the proximal tubule and thick ascending limb (TAL). The residual K^+ is passed along to the collecting ducts where K^+ is added prior to excretion as urine. The addition of K^+ in the collecting ducts occurs transcellularly, via ROMK channels in principal cells and BK channels in intercalated cells (McDonough and Youn, 2017). Although we expect K^+ channels to be associated with a large K isotope effect (ε_{ch} = 1.2‰), the extent to which this determines the $\delta^{41}K_{plasma}$ value of urine depends on 1) the $\delta^{41}K_{plasma}$ value of the residual K^+ exiting the TAL (after reabsorption but before secretion) and 2) internal K^+ cycling within the principal and intercalated cells (e.g. eqn (3)). The observation that $\varepsilon_{\mathrm{kidney}}$ is only ~ $0.50‰$ suggests that either the residual K^+ exiting the TAL has an elevated $\delta^{41}K_{plasma}$ value due to preferential removal of ^{39}K during reabsorption and/or the $\delta^{41}K_{plasma}$ value of ICF in principal and intercalated cells elevated, for example due to high values of Δf_{ch}.

4.3.2.2 Cerebrospinal fluid (CSF). K^+ in CSF reflects a balance between paracellular and transcellular K^+ transport across endothelial cells at the blood-brain-barrier (BBB) and paracellular K^+ transport of across epithelial cells of the choroid plexus (Hladky and Barrand, 2016). Gross fluxes of K^+ into the brain across the BBB are 4x larger than those associated with the choroid plexus (Katzman et al., 1965), suggesting that the observed net K isotope effects may be largely due to fractionation associated with transport across the BBB. However, K^+ transport from ECF to CSF through the choroid plexus is thought to occur by paracellular routes through pores in tight junctions (Figure 4), a process that we expect to fractionate K isotopes and thus may contribute to the observed negative $\delta^{41}K_{plasma}$ values for CSF. With regards to K^+ transport across the BBB, both paracellular (through tight-junction pores) and transcellular (through BBB endothelial cells) routes may be important (Hladky and Barrand, 2016). Again, we expect paracellular K^+ transport through tight junction pores to be associated with a larger K isotope effect whereas any K isotope effects associated with transcellular transport will depend on the internal cycling of K^+ (and associated isotope effects) within endothelial BBB cells (pumps, (Betz et al., 1980); co-transporters, (Foroutan et al., 2005); and channels, (Van Renterghem et al., 1995)). Overall, the observation of large K isotope fractionation associated with the transport of K^+ from plasma to CSF (Fig. 5; $\varepsilon_{\mathrm{CSF}} = 0.59 \pm 0.12‰$) requires that either 1) there is a large K isotope effect associated with transcellular K^+ transport across endothelial BBB cells or 2) transport of K^+ from plasma to CSF is dominated by paracellular routes in both the choroid plexus and across the BBB.

4.4 Stenohaline and Euryhaline Marine Fish. K^+ homeostasis in both euryhaline and stenohaline marine fish is linked to ionic and osmotic regulation (Figure 5). While K^+ sources include ingestion of seawater and diet (Hickman Jr, 1968), by far the largest K^+ source is transport across the gills (Maetz, 1969), which are permeable to monovalent cations (Na^+, K^+) and anions (Cl^-). Fish balance this salt intake by actively secreting Na^+, K^+ and Cl^- through mitochondria-rich cells (MRCs) of the gills and paracellularly through tight-junction proteins (claudins) in the gill epithelium (Evans et al., 2005; Kolosov et al., 2013). K^+ loss is not well-understood but recent discoveries of apical ROMK channels indicate that transcellular secretion through MRCs is likely an important pathway (Furukawa et al., 2012). Both stenohaline and euryhaline marine fish possess this capability but euryhaline marine fish have evolved the ability to adapt this machinery to a wide range of water salinities by adjusting expression of ROMK and tight junction claudins (Furukawa et al., 2012; Furukawa et al., 2014; Furukawa et al., 2015; Kolosov et al., 2013).

In seawater adapted stenohaline and euryhaline marine fish, K^+ homeostasis can be approximated as a balance between gain of K^+ across tight-junctions in the gill epithelium and loss of K^+ through apical ROMK channels in MRCs (Figure 5b). Other potential sources and sinks of K^+ including the ingestion of seawater, diet, and excretion are either small compared to the fluxes of K^+ across the gills (Maetz, 1969) or transient in nature and unlikely to explain the systematic difference we observe between the $\delta^{41}K_{seawater}$ values of stenohaline and euryhaline fish. Furthermore, as most of the total K^+ content of fish resides in muscle tissue, the $\delta^{41}K_{seawater}$ value of the muscle can be used as a reasonable approximation of the $\delta^{41}K_{seawater}$ value of the whole organism (Figure 5b). At steady-state ($\mathrm{F}_{\mathrm{gill}}^{in} = \mathrm{F}_{\mathrm{MRC}}^{out}$), the $\delta^{41}K_{seawater}$ value of the whole organism will reflect the balance between K isotope fractionation associated with K^+ sources (paracellular transport across the gills, $\varepsilon_{\mathrm{gill}}$) and K^+ sinks (transcellular transport through ROMK channels in MRCs, $\varepsilon_{\mathrm{ch}}$):

$$(\delta^{41}K_{seawater} - \varepsilon_{\mathrm{gill}}) \cdot \mathrm{F}_{\mathrm{gill}}^{in} = (\delta^{41}K_{MRC} - \varepsilon_{\mathrm{ch}}) \cdot \mathrm{F}_{\mathrm{MRC}}^{out} \quad (5)$$

which reduces to:

$$\delta^{41}K_{seawater}^{MRC} = (\varepsilon_{\mathrm{ch}} - \varepsilon_{\mathrm{gill}}) \quad (5a)$$

where $\delta^{41}K_{seawater}^{MRC}$ is the difference between the $\delta^{41}K$ value of the MRCs and seawater. The $\delta^{41}K$ value of MRCs can be related to the $\delta^{41}K$ value of the whole fish by combining equation (5a) with equation (3) and assuming 1) that the flux of K^+ out of MRCs via apical ROMK channels is small compared to the gross fluxes of K^+ into/out of MRCs associated with K homeostasis and 2) the $\delta^{41}K$ value of plasma is similar to

514 muscle (a reasonable assumption for most muscles in *R. norvegicus*, Figure 3b) . In this
515 case:

516 $$\delta^{41}K_{seawater}^{plasma/muscle} = (\varepsilon_{ch} - \varepsilon_{gill}) - \Delta f_{ch} \cdot (\varepsilon_{ch} - \varepsilon_{p/co}) \quad (6)$$

517 where Δf_{ch} is the relative difference in K loss via channels in MRCs. Although we do not
518 independently know the value of ε_{gill} and suspect that it may vary systematically between
519 stenohaline and euryhaline marine fish, we speculate that ~0.2 to 1.2‰ represents a
520 plausible range based on results for epithelial cells in the gut of *R. norvegicus* (Figure
521 3b) and the maximum K isotope fractionation expected for channels (ε_{ch}). Values of ε_{ch}
522 and $\varepsilon_{p/co}$ are assumed to be 1.2‰, and 0‰, respectively. Given these values, inspection
523 of equation (6) indicates both positive and negative $\delta^{41}K_{seawater}^{plasma/muscle}$ are possible. For
524 example, as $\Delta f_{ch} \to 0$, $\delta^{41}K_{seawater}^{plasma/muscle} \to (\varepsilon_{ch} - \varepsilon_{gill})$ a result which yields $\delta^{41}K_{seawater}^{plasma/muscle} = 0$
525 to +1‰, in agreement with measured $\delta^{41}K_{seawater}^{plasma/muscle}$ values in euryhaline marine fish.
526 Alternatively, as $\Delta f_{ch} \to 1$, $\delta^{41}K_{seawater}^{plasma/muscle} \to (\varepsilon_{p/co} - \varepsilon_{gill})$ a result which yields
527 $\delta^{41}K_{seawater}^{plasma/muscle}$ = -0.2 to -1.2‰, in agreement with measured $\delta^{41}K_{seawater}^{plasma/muscle}$ values in
528 stenohaline marine fish.

529 But is there any independent evidence that K homeostasis in MRCs in
530 stenohaline marine fish operates close to a perfect 'pump-leak' ($\Delta f_{ch} \sim 1$) mechanism
531 whereas the MRCs of euryhaline marine fish operate much closer to a 'leak-leak' or
532 'pump-pump' mechanism ($\Delta f_{ch} \sim 0$)? The gill epithelium of stenohaline marine fish is
533 considered to be more permeable than stenohaline freshwater fish due to the presence
534 of tight-junctions connecting gill accessory cells with MRCs (Chasiotis et al., 2012). This
535 increased permeability to NaCl must be balanced by increased NaCl secretion, a
536 process that has been shown to be linked to the activity of $NaKATP_{ase}$ in MRCs;
537 activities of $NaKATP_{ase}$ is higher in marine species than freshwater species and increase
538 when euryhaline species are acclimated to seawater (Epstein et al., 1967; Jampol and
539 Epstein, 1970). As an increase in the activity of $NaKATP_{ase}$ activity will, all else held
540 constant, lower f_{ch}^{in} and increase Δf_{ch}, one way of interpreting the apparent difference in
541 Δf_{ch} between MRCs of stenohaline and euryhaline marine fish is that the more
542 permeable gills of stenohaline marine fish require greater NaCl secretion and higher
543 activities of $NaKATP_{ase}$ in MRCs (e.g. Figure 3c).

544 *5. Conclusions:* The results presented here demonstrate that K^+ homeostasis in
545 biological systems is associated with systematic variability in $^{41}K/^{39}K$ ratios and strongly
546 suggests that K^+ transport through channels and tight-junction proteins is associated
547 with greater fractionation of K isotopes than transport via pumps and co-transporters.
548 Using results from 3 biological systems (algae, mammals, and fish) we developed a
549 simple framework for interpreting differences in measured $\delta^{41}K$ values between

intercellular fluid (ICF) and extracellular fluid (ECF) and between different internal fluid reservoirs (e.g. blood plasma and cerebrospinal fluid). If correct, this framework permits quantification of the relative importance of K^+ channels and pump/cotransporters in different physiological states – e.g. K depletion/excess - *in situ* (e.g $\delta^{41}K_{plasma}^{heart}$) and in some cases *in vivo* (e.g $\delta^{41}K_{plasma}^{urine}$). However, with the exception of *C. Reinhardtii* where the observed isotopic difference between media and the whole cell can be attributed to a single transport mechanism, our results do not directly constrain the magnitude of the individual K isotope effects associated with the machinery of K^+ transport. Quantifying machinery-specific K isotope effects through a combination of laboratory and numerical approaches (14) is therefore a high-priority for future research.

Data Availability Statement. The data that support the findings of this study are available in the methods and/or supplementary material of this article.

Conflict of Interest Statement. The authors declare no conflict of interest.

Author Contributions JAH, AAM, JHY, DPS, and CS designed the research. JAH, DPS, DH, SK, SG, and CS carried out the experiments and associated analytical measurements. JAH, AAM, JHY, DPS, and CS interpreted the data and wrote the manuscript. All authors were involved in the revising of the manuscript.

Acknowledgments

Cornelia Spetea acknowledges the sabbatical program at the Faculty of Science, University of Gothenburg, and thanks Martin C. Jonikas for the *Chlamydomonas* experiments performed in his laboratory at Princeton University. John Higgins, Alicia McDonough, and Jang Youn thank the University Kidney Research Organization (UKRO) for financial support. Anne Pearson is thanked for helpful reviews on an earlier version of this manuscript.

References

Agarwal R., Afzalpurkar R. and Fordtran J. S. (1994) Pathophysiology of potassium absorption and secretion by the human intestine. *Gastroenterology* **107**, 548-571.

Barnaby C. F. and Edmonds C. J. (1969) Use of a miniature GM counter and a whole body counter in the study of potassium transport by the colon of normal, sodium-depleted and adrenalectomized rats in vivo. *J Physiol* **205**, 647-665.

Berneche S. and Roux B. (2003) A microscopic view of ion conduction through the K+ channel. *Proceedings of the National Academy of Sciences of the United States of America* **100**, 8644-8648.

Betz A. L., Firth J. A. and Goldstein G. W. (1980) Polarity of the blood-brain barrier: distribution of enzymes between the luminal and antiluminal membranes of brain capillary endothelial cells. *Brain research* **192**, 17-28.

Boron W. F., Boulpaep, E.L. (2005) *Medical Physiology*. Elsevier Saunders, Philadelphia, Pennsylvania.

595 Bradbury M. and Davson H. (1965) The transport of potassium between blood,
596 cerebrospinal fluid and brain. *The Journal of physiology* **181**, 151-174.
597 Britto D. T. and Kronzucker H. J. (2008) Cellular mechanisms of potassium transport in
598 plants. *Physiologia Plantarum* **133**, 637-650.
599 Chasiotis H., Kolosov D., Bui P. and Kelly S. (2012) Tight junctions, tight junction
600 proteins and paracellular permeability across the gill epithelium of fishes: A
601 review. *Respiratory physiology & neurobiology* **184**.
602 Christensen J. N., Qin L., Brown S. T. and DePaolo D. J. (2018) Potassium and calcium
603 isotopic fractionation by plants (soybean [Glycine max], rice [Oryza sativa], and
604 wheat [Triticum aestivum]). *ACS Earth and Space Chemistry* **2**, 745-752.
605 Duhm J. (1987) Furosemide-sensitive K+ (Rb+) transport in human-erythrocytes - modes
606 of operation, dependence on extracellular and intracellular Na+, kinetics, pH
607 dependency, and the effect of cell-volume and N-ethylmaleimide. *J. Membr. Biol.*
608 **98**, 15-32.
609 Epstein E., Rains D. and Elzam O. (1963) Resolution of dual mechanisms of potassium
610 absorption by barley roots. *Proceedings of the National Academy of Sciences of*
611 *the United States of America* **49**, 684.
612 Epstein F. H., Katz A. I. and Pickford G. E. (1967) Sodium- and potassium-activated
613 adenosine triphosphatase of gills: role in adaptation of teleosts to salt water.
614 *Science* **156**, 1245-1247.
615 Evans D. H., Piermarini P. M. and Choe K. P. (2005) The multifunctional fish gill:
616 dominant site of gas exchange, osmoregulation, acid-base regulation, and
617 excretion of nitrogenous waste. *Physiological reviews* **85**, 97-177.
618 Foroutan S., Brillault J., Forbush B. and O'Donnell M. E. (2005) Moderate-to-severe
619 ischemic conditions increase activity and phosphorylation of the cerebral
620 microvascular endothelial cell Na+-K+-Cl− cotransporter. *American Journal of*
621 *Physiology-Cell Physiology* **289**, C1492-C1501.
622 Foster E. S., Hayslett J. P. and Binder H. J. (1984) Mechanism of active potassium
623 absorption and secretion in the rat colon. *Am J Physiol* **246**, G611-617.
624 Franco R. S., Puchulu-Campanella M. E., Barber L. A., Palascak M. B., Joiner C. H.,
625 Low P. S. and Cohen R. M. (2013) Changes in the properties of normal human
626 red blood cells during in vivo aging. *American Journal of Hematology* **88**, 44-51.
627 Furukawa F., Watanabe S., Kimura S. and Kaneko T. (2012) Potassium excretion through
628 ROMK potassium channel expressed in gill mitochondrion-rich cells of
629 Mozambique tilapia. *American Journal of Physiology-Regulatory, Integrative and*
630 *Comparative Physiology* **302**, R568-R576.
631 Furukawa F., Watanabe S., Kakumura K., Hiroi J. and Kaneko T. (2014) Gene
632 expression and cellular localization of ROMKs in the gills and kidney of
633 Mozambique tilapia acclimated to fresh water with high potassium concentration.
634 *American Journal of Physiology-Regulatory, Integrative and Comparative*
635 *Physiology* **307**, R1303-R1312.
636 Furukawa F., Watanabe S., Seale A. P., Breves J. P., Lerner D. T., Grau E. G. and
637 Kaneko T. (2015) In vivo and in vitro effects of high-K+ stress on branchial
638 expression of ROMKa in seawater-acclimated Mozambique tilapia. *Comparative*

639 *Biochemistry and Physiology Part A: Molecular & Integrative Physiology* **187**,
640 111-118.
641 Garcia-Hernandez V., Quiros M. and Nusrat A. (2017) Intestinal epithelial claudins:
642 expression and regulation in homeostasis and inflammation. *Ann. N.Y. Acad. Sci.*
643 **1397**, 66-79.
644 Gardos G. (1958) The function of calcium in the potassium permeability of human
645 erythrocytes. *Biochimica et biophysica acta* **30**, 653-654.
646 Gaymard F., Pilot G., Lacombe B., Bouchez D., Bruneau D., Boucherez J., Michaux-
647 Ferriere N., Thibaud J.-B. and Sentenac H. (1998) Identification and disruption of
648 a plant shaker-like outward channel involved in K+ release into the xylem sap.
649 *Cell* **94**, 647-655.
650 Gick G. G., Hatala M. A., Chon D. and Ismail-Beigi F. (1993) Na,K-ATPase in several
651 tissues of the rat: Tissue-specific expression of subunit mRNAs and enzyme
652 activity. *The Journal of Membrane Biology* **131**, 229-236.
653 Gierth M. and Mäser P. (2007) Potassium transporters in plants–involvement in K+
654 acquisition, redistribution and homeostasis. *FEBS letters* **581**, 2348-2356.
655 Hibino H., Inanobe A., Furutani K., Murakami S., Findlay I. and Kurachi Y. (2010)
656 Inwardly rectifying potassium channels: their structure, function, and
657 physiological roles. *Physiol Rev* **90**, 291-366.
658 Hickman Jr C. P. (1968) Ingestion, intestinal absorption, and elimination of seawater and
659 salts in the southern flounder, Paralichthys lethostigma. *Canadian journal of*
660 *zoology* **46**, 457-466.
661 Hirsch R. E., Lewis B. D., Spalding E. P. and Sussman M. R. (1998) A role for the AKT1
662 potassium channel in plant nutrition. *Science* **280**, 918-921.
663 Hladky S. B. and Barrand M. A. (2016) Fluid and ion transfer across the blood–brain and
664 blood–cerebrospinal fluid barriers; a comparative account of mechanisms and
665 roles. *Fluids and Barriers of the CNS* **13**, 1-69.
666 Hofmann A. E., Bourg I. C. and DePaolo D. J. (2012) Ion desolvation as a mechanism for
667 kinetic isotope fractionation in aqueous systems. *Proceedings of the National*
668 *Academy of Sciences* **109**, 18689-18694.
669 Jampol L. M. and Epstein F. H. (1970) Sodium-potassium-activated adenosine
670 triphosphatase and osmotic regulation by fishes. *American Journal of Physiology-*
671 *Legacy Content* **218**, 607-611.
672 Jones A. W., Sander P. D. and Kampschmidt D. L. (1977) The effect of norepinephrine
673 on aortic 42K turnover during deoxycorticosterone acetate hypertension and
674 antihypertensive therapy in the rat. *Circulation research* **41**, 256-260.
675 Katzman R., Graziani L., Kaplan R. and Escriva A. (1965) Exchange of cerebrospinal
676 fluid potassium with blood and brain: study in normal and ouabain perfused cats.
677 *Archives of neurology* **13**, 513-524.
678 Kochian L. V. and Lucas W. J. (1982) Potassium transport in corn roots: I. Resolution of
679 kinetics into a saturable and linear component. *Plant Physiology* **70**, 1723-1731.
680 Kolosov D., Bui P., Chasiotis H. and Kelly S. P. (2013) Claudins in teleost fishes. *Tissue*
681 *barriers* **1**, e25391.

682 Kopec W., Köpfer D. A., Vickery O. N., Bondarenko A. S., Jansen T. L., De Groot B. L.
683 and Zachariae U. (2018) Direct knock-on of desolvated ions governs strict ion
684 selectivity in K+ channels. *Nature chemistry* **10**, 813-820.
685 Lacombe B., Pilot G., Michard E., Gaymard F., Sentenac H. and Thibaud J.-B. (2000) A
686 shaker-like K+ channel with weak rectification is expressed in both source and
687 sink phloem tissues of Arabidopsis. *The Plant Cell* **12**, 837-851.
688 Lebaudy A., Véry A.-A. and Sentenac H. (2007) K+ channel activity in plants: genes,
689 regulations and functions. *FEBS letters* **581**, 2357-2366.
690 Li W., Kwon K. D., Li S. and Beard B. L. (2017) Potassium isotope fractionation
691 between K-salts and saturated aqueous solutions at room temperature: Laboratory
692 experiments and theoretical calculations. *Geochimica et Cosmochimica Acta* **214**,
693 1-13.
694 MacKinnon R. (2003) Potassium channels. *FEBS Letters* **555**, 62-65.
695 Maetz J. (1969) Seawater teleosts - evidence for a sodium-potassium exchange in
696 branchial sodium-excreting pump. *Science* **166**, 613-&.
697 Malhotra B. and Glass A. D. (1995) Potassium fluxes in Chlamydomonas reinhardtii (I.
698 Kinetics and electrical potentials). *Plant physiology* **108**, 1527-1536.
699 Marchand J., Heydarizadeh P., Schoefs B. and Spetea C. (2020) Chloroplast Ion and
700 Metabolite Transport in Algae. In *Photosynthesis in Algae: Biochemical and*
701 *Physiological Mechanisms* (eds. A. W. D. Larkum, A. R. Grossman and J. A.
702 Raven). Springer International Publishing, Cham. pp. 107-139.
703 McDonough A. A. and Youn J. H. (2017) Potassium Homeostasis: The Knowns, the
704 Unknowns, and the Health Benefits. *Physiology (Bethesda)* **32**, 100-111.
705 Mironenko A., Zachariae U., de Groot B. L. and Kopec W. (2021) The Persistent
706 Question of Potassium Channel Permeation Mechanisms. *Journal of Molecular*
707 *Biology* **433**, 167002.
708 Morgan L. E., Ramos D. P. S., Davidheiser-Kroll B., Faithfull J., Lloyd N. S., Ellam R.
709 M. and Higgins J. A. (2018) High-precision K-41/K-39 measurements by MC-
710 ICP-MS indicate terrestrial variability of delta K-41. *Journal of Analytical Atomic*
711 *Spectrometry* **33**, 175-186.
712 Mulkidjanian A. Y., Bychkov A. Y., Dibrova D. V., Galperin M. Y. and Koonin E. V.
713 (2012) Origin of first cells at terrestrial, anoxic geothermal fields. *Proceedings of*
714 *the National Academy of Sciences* **109**, E821-E830.
715 Noble E. E., Hahn J. D., Konanur V. R., Hsu T. M., Page S. J., Cortella A. M., Liu C. M.,
716 Song M. Y., Suarez A. N., Szujewski C. C., Rider D., Clarke J. E., Darvas M.,
717 Appleyard S. M. and Kanoski S. E. (2018) Control of Feeding Behavior by
718 Cerebral Ventricular Volume Transmission of Melanin-Concentrating Hormone.
719 *Cell Metab* **28**, 55-68 e57.
720 Pilot G., Lacombe B. t., Gaymard F., Chérel I., Boucherez J., Thibaud J.-B. and Sentenac
721 H. (2001) Guard cell inward K+ channel activity inarabidopsis involves
722 expression of the twin channel subunits KAT1 and KAT2. *Journal of Biological*
723 *Chemistry* **276**, 3215-3221.
724 Ramos D. P. S., Morgan L. E., Lloyd N. S. and Higgins J. A. (2018) Reverse weathering
725 in marine sediments and the geochemical cycle of potassium in seawater: Insights

from the K isotopic composition (K-41/K-39) of deep-sea pore-fluids. *Geochimica Et Cosmochimica Acta* **236**, 99-120.

Ramos D. P. S., Coogan L. A., Murphy J. G. and Higgins J. A. (2020) Low-temperature oceanic crust alteration and the isotopic budgets of potassium and magnesium in seawater. *Earth and Planetary Science Letters* **541**, 11.

Rolfe D. F. and Brown G. C. (1997) Cellular energy utilization and molecular origin of standard metabolic rate in mammals. *Physiol Rev* **77**, 731-758.

Roux B. (2017) Ion channels and ion selectivity. *Essays in biochemistry* **61**, 201-209.

Rui H., Artigas P. and Roux B. (2016) The selectivity of the Na+/K+-pump is controlled by binding site protonation and self-correcting occlusion. *Elife* **5**, e16616.

Sachs J. R. (1971) Ouabain-insensitive sodium movements in human red blood cell. *Journal of General Physiology* **57**, 259-&.

Stautz J., Hellmich Y., Fuss M. F., Silberberg J. M., Devlin J. R., Stockbridge R. B. and Haenelt I. (2021) Molecular Mechanisms for Bacterial Potassium Homeostasis. *Journal of Molecular Biology* **433**.

Terner C., Eggleston L. and Krebs H. (1950) The role of glutamic acid in the transport of potassium in brain and retina. *Biochemical Journal* **47**, 139.

Tosteson D. C. and Hoffman J. F. (1960) Regulation of cell volume by active cation transport in high and low potassium sheep red cells. *Journal of General Physiology* **44**, 169-194.

Van Renterghem C., Vigne P. and Frelin C. (1995) A charybdotoxin-sensitive, Ca2+-activated K+ channel with inward rectifying properties in brain microvascular endothelial cells: properties and activation by endothelins. *Journal of neurochemistry* **65**, 1274-1281.

Wang K. and Jacobsen S. B. (2016) An estimate of the Bulk Silicate Earth potassium isotopic composition based on MC-ICPMS measurements of basalts. *Geochimica Et Cosmochimica Acta* **178**, 223-232.

Youn J. H. and McDonough A. A. (2009) Recent advances in understanding integrative control of potassium homeostasis. *Annual review of physiology* **71**, 381-401.

Yu H., Noskov S. Y. and Roux B. (2010) Two mechanisms of ion selectivity in protein binding sites. *Proceedings of the National Academy of Sciences* **107**, 20329-20334.

Zeng H., Rozsa V. F., Nie N. X., Zhang Z., Pham T. A., Galli G. and Dauphas N. (2019) Ab Initio Calculation of Equilibrium Isotopic Fractionations of Potassium and Rubidium in Minerals and Water. *Acs Earth and Space Chemistry* **3**, 2601-2612.

Table S1.

C. Reinardtii

Sample ID	$\delta^{41}K_{medium}$	2 S.E.	N	K (pg/cell)	Notes
TP Medium	0	0.1	3		Tris Phosphate (TP) growth medium
Wild Type 1	-1.14	0.06	3	0.258	wild type
Wild Type 2	-1.1	0.14	3	0.278	wild type
Cre50 mutant	-1.24	0.18	3	0.210	mitrochondrial Mg transport mutant

Stenohaline and Euryhaline Marine Teleosts

Sample ID	Type	Source	$[K^+]$ mM	K/Na (g/g)	$\delta^{41}K_{seawater}$	2σ / 2 S.E.	N
Oncorhynchus kisutch_1	Euryhaline	Nassau Seafood, Princeton, NJ	85	2.50	0.27	0.17	1
Oncorhynchus kisutch_2	Euryhaline	Fulton Fish Market, NY, NY	84	1.87	0.63	0.11	2
Oncorhynchus kisutch_3	Euryhaline	Fulton Fish Market, NY, NY	87	2.02	0.93	0.17	1
Oncorhynchus tshawytscha_1	Euryhaline	Nassau Seafood, Princeton, NJ	79	3.76	-0.1	0.17	1
Oncorhynchus tshawytscha_2	Euryhaline	Fulton Fish Market, NY, NY	74	2.44	0.2	0.17	1
Oncorhynchus tshawytscha_3	Euryhaline	Nassau Seafood, Princeton, NJ			0.17	0.17	1
Oncorhynchus nerka_1	Euryhaline	Trader Joe's, Princeton, NJ	89	2.50	0.22	0.17	1
Oncorhynchus nerka_2	Euryhaline	Fulton Fish Market, NY, NY	99	1.87	0.25	0.17	1
Oncorhynchus nerka_3	Euryhaline	Fulton Fish Market, NY, NY	106	2.02	0.2	0.13	2
Oncorhynchus nerka_4	Euryhaline	Fulton Fish Market, NY, NY	111	3.76	0.12	0.17	1
Gadus morhua_1	Stenohaline	NOAA Cruise ID201504	92	2.50	-0.64	0.05	4
Gadus morhua_2	Stenohaline	NOAA Cruise ID201504	100	1.87	-0.47	0.05	3
Gadus morhua_3	Stenohaline	Fulton Fish Market, NY, NY	102	2.02	-0.54	0.06	2
Gadus morhua_4	Stenohaline	Fulton Fish Market, NY, NY	105	3.76	-0.68	0.04	2
Peprilus striacanthus_1	Stenohaline	NOAA Cruise ID201504	128	2.50	-0.72	0.04	2
Peprilus striacanthus_2	Stenohaline	NOAA Cruise ID201504	152	1.87	-0.48	0.16	2
Peprilus striacanthus_3	Stenohaline	NOAA Cruise ID201504	124	2.02	-0.7	0.17	1
Peprilus striacanthus_4	Stenohaline	NOAA Cruise ID201504	112	3.76	-0.33	0.17	1
Xiphias gladius_1	Stenohaline	Trader Joe's, Princeton, NJ	99	2.50	-0.58	0.17	1
Xiphias gladius_2	Stenohaline	Trader Joe's, Princeton, NJ	104	1.87	-0.32	0.04	2

Xiphias gladius_3	Stenohaline	Fulton Fish Market, NY, NY	109	2.02	-0.55	0.17	1
Xiphias gladius_4	Stenohaline	Fulton Fish Market, NY, NY	113	3.76	-0.74	0.17	1
Pseudopleuronectes americanus_1	Stenohaline	NOAA Cruise ID201504	139	2.50	-0.39	0.05	2
Pseudopleuronectes americanus_2	Stenohaline	NOAA Cruise ID201504	121	1.87	-0.68	0.01	2
Pseudopleuronectes americanus_3	Stenohaline	NOAA Cruise ID201504	137	2.02	-0.37	0.17	1
Pseudopleuronectes americanus_4	Stenohaline	NOAA Cruise ID201504	134	3.76	-0.47	0.17	1
Pseudopleuronectes americanus_5	Stenohaline	NOAA Cruise ID201504	124	2.44	-0.36	0.17	1
Hippoglossus stenolepis_1	Stenohaline	Fulton Fish Market, NY, NY	132	3.76	-0.62	0.17	1
Hippoglossus stenolepis_2	Stenohaline	Fulton Fish Market, NY, NY	116	2.44	-0.97	0.04	2
Hippoglossus stenolepis_3	Stenohaline	Nassau Seafood, Princeton, NJ			-1.02	0.17	1

767

768 *R. norvegicus (no brain)*

Sample	$\delta^{41}K_{diet}$	$\delta^{41}K_{plasma}$	2σ / 2 S.E.	N	$[K^+]$ mM	K/Na (mol/mol)
$Diet_{average}$	**0.00**	**-0.35**	**0.04**	**10**		
$Urine_1$	-0.08	-0.43	0.06	6	381	1.60
$Urine_2$	-0.06	-0.59	0.01	2	280	1.97
$Urine_3$	-0.12	-0.47	0.05	8	216	2.02
$Urine_{average}$	**-0.09**	**-0.50**	**0.10**	**3**	**293**	**1.80**
$Feces_1$	0.25	-0.10	0.05	2		
$Feces_2$	0.22	-0.31	0.06	2		
$Feces_3$	0.11	-0.24	0.17	1		
$Feces_{average}$	**0.19**	**-0.22**	**0.12**	**3**		
$Plasma_1$	0.35	0.00	0.06	3	3.95	0.03
$Plasma_2$	0.53	0.00	0.03	4	4.13	0.03
$Plasma_3$	0.35	0.00	0.04	6	6.77	0.05
$Plasma_{average}$	**0.41**	**0.00**	**0.12**	**3**	**4.95**	**0.04**
Red blood $cells_1$	0.81	0.46	0.07	2	102	7.23
Red blood $cells_2$	0.93	0.40	0.03	5	92	6.02
Red blood $cells_3$	0.68	0.33	0.08	3	95	6.46
Red blood $cells_{average}$	**0.81**	**0.40**	**0.08**	**3**	**96**	**6.56**
$Heart_1$	1.05	0.70	0.14	2	74	1.07
$Heart_2$	0.99	0.46	0.01	2	78	1.41
$Heart_3$	0.84	0.49	0.06	2	79	1.24
$Heart_{average}$	**0.96**	**0.55**	**0.15**	**3**	**77**	**1.23**
$Liver_1$	0.69	0.34	0.03	2	95	3.81
$Liver_2$	0.85	0.32	0.04	2	82	2.57
$Liver_3$	0.60	0.25	0.03	4	98	3.16
$Liver_{average}$	**0.71**	**0.30**	**0.05**	**3**	**92**	**3.13**
$Soleus_1$	0.49	0.14	0.01	2	104	3.10
$Soleus_2$	0.71	0.18	0.04	5	93	3.23
$Soleus_3$	0.54	0.19	0.03	4	101	3.20
$Soleus_{average}$	**0.58**	**0.17**	**0.03**	**3**	**100**	**3.17**

TA_1	0.34	-0.01	0.11	2	116	4.18
TA_2	0.64	0.11	0.02	2	120	3.82
TA_3	0.51	0.16	0.05	3	113	3.15
$TA_{average}$	**0.50**	**0.09**	**0.10**	**3**	**117**	**3.67**
EDL_1	0.53	0.18	0.10	3		
EDL_2	0.60	0.07	0.07	2	104	4.14
EDL_3	0.61	0.26	0.04	3	107	3.63
$EDL_{average}$	**0.58**	**0.17**	**0.11**	**3**	**106**	**3.86**
$Gastrocnemius_1$	0.48	0.13	0.03	2	120	5.07
$Gastrocnemius_2$	0.56	0.03	0.05	2	117	3.74
$Gastrocnemius_3$	0.22	-0.13	0.07	2	118	4.20
$Gastroc_{average}$	**0.42**	**0.01**	**0.15**	**3**	**118**	**4.28**
$Stomach_1$	0.54	0.19	0.10	2		
$Stomach_2$	0.52	-0.01	0.03	2		
$Stomach_3$	0.39	0.04	0.06	3		
$Stomach_{average}$	**0.48**	**0.07**	**0.12**	**3**		
$Kidney_1$	0.42	0.07	0.07	2		
$Kidney_2$	0.66	0.13	0.04	2		
$Kidney_3$	0.36	0.01	0.07	2		
$Kidney_{average}$	**0.48**	**0.07**	**0.07**	**3**		
Adipose $tissue_1$	0.44	0.09	0.10	2		
Adipose $tissue_2$	0.49	-0.04	0.07	2		
Adipose $tissue_3$	0.33	-0.02	0.17	1		
Adipose $tissue_{average}$	**0.42**	**0.01**	**0.08**	**3**		

R. norvegicus (brain)

Sample	$\delta^{41}K_{diet}$	$\delta^{41}K_{plasma}$	$\delta^{41}K_{CSF}$	2 S.E.	N
$Plasma_1$	0.36	0.00	0.54	0.05	4
$Plasma_2$	0.38	0.00	0.56	0.12	5
$Plasma_3$	0.59	0.00	0.77	0.14	3
$Plasma_4$	0.33	0.00	0.51	0.1	6
$Plasma_{average}$	**0.41**	**0.00**	**0.59**	**0.12**	**4**
Cerebrospinal fluid $(CSF)_1$	-0.13	-0.54	0.00	0.07	4
Cerebrospinal fluid $(CSF)_2$	-0.15	-0.56	0.00	0.18	4
Cerebrospinal fluid $(CSF)_3$	-0.36	-0.77	0.00	0.09	3
Cerebrospinal fluid $(CSF)_4$	-0.10	-0.51	0.00	0.15	4
Cerebrospinal fluid $(CSF)_{average}$	**-0.18**	**-0.59**	**0.00**	**0.12**	**4**
$Cerebellum_1$	0.06	-0.35	0.19	0.09	4
$Cerebellum_2$	-0.07	-0.48	0.09	0.15	4
$Cerebellum_3$	0.00	-0.41	0.36	0.04	7
$Cerebellum_4$	0.12	-0.29	0.21	0.12	5
$Cerebellum_{average}$	**0.03**	**-0.38**	**0.21**	**0.11**	**4**
Spinal $cord_1$	0.01	-0.40	0.14	0.07	6
Spinal $cord_2$	0.04	-0.37	0.20	0.06	6
Spinal $cord_3$	0.16	-0.25	0.52	0.1	6
Spinal $cord_4$	0.23	-0.18	0.33	0.09	7
Spinal $cord_{average}$	**0.11**	**-0.30**	**0.30**	**0.17**	**4**
$Cerebrum_1$	0.26	-0.15	0.39	0.07	6
$Cerebrum_2$	0.11	-0.30	0.26	0.05	6
$Cerebrum_3$	0.17	-0.24	0.53	0.09	6
$Cerebrum_4$	0.08	-0.33	0.18	0.09	3
$Cerebrum_{average}$	**0.16**	**-0.25**	**0.34**	**0.15**	**4**

Figures.

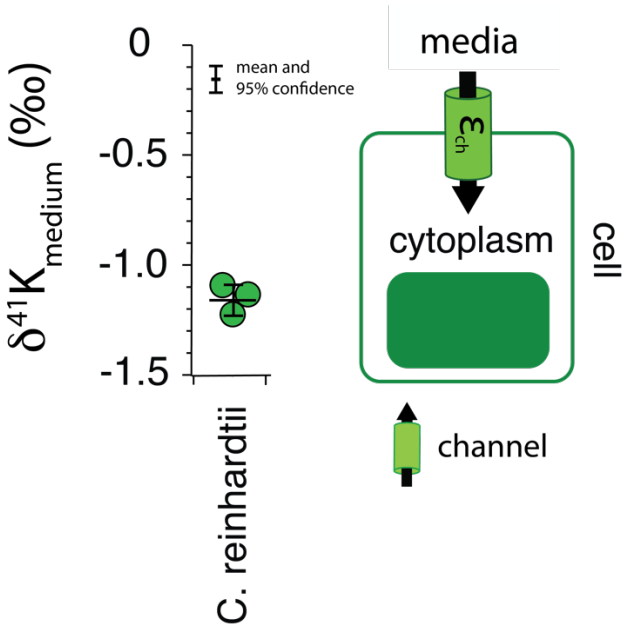

Figure 1. The difference in $\delta^{41}K$ values between external and intracellular K^+ in growth experiments of *C. reinhardtii* and a diagram of K^+ transport in single-celled algae grown under optimal conditions (See Methods) where K uptake occurs via channels that fractionate K isotopes (ε_{ch}) by ~1.2‰ . $P = 4.5 \times 10^{-5}$ by one-way ANOVA in Matlab.

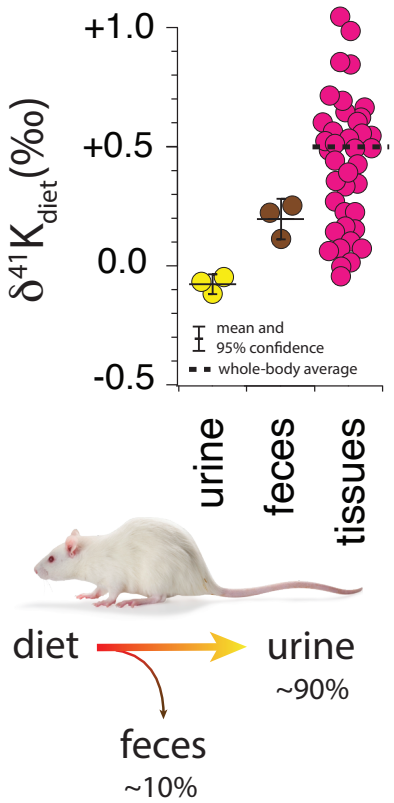

Figure 2. Whole-body K isotope mass balance in *R. norvegicus* on a controlled diet. Measured $\delta^{41}K$ values of urine ($P = 0.19$) and feces ($P = 0.037$) relative to diet indicate a preferential uptake of ^{39}K in the gut. The total range in $\delta^{41}K_{diet}$ values in the tissues of *R. norvegicus* is ~1‰ with an estimated whole-body average $\delta^{41}K_{diet}$ value of approx. +0.5‰, consistent with preferential loss of ^{39}K in urine.

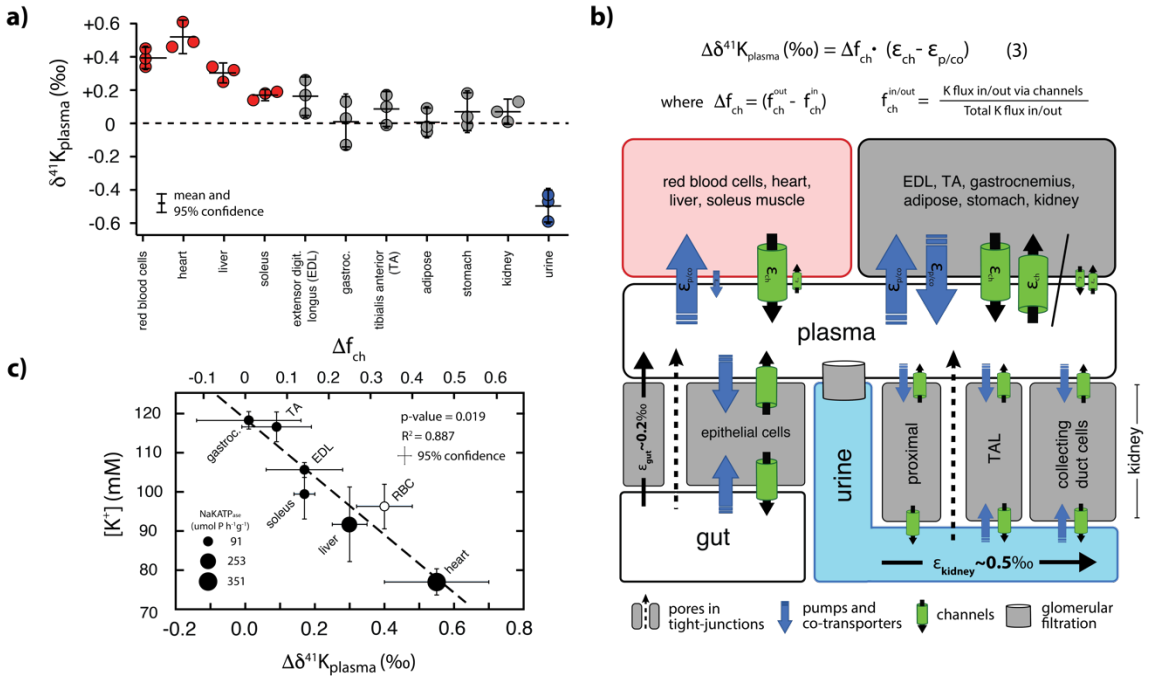

Figure 3. a) K isotopic composition of tissues/fluids *Rattus norvegicus* normalized to plasma ($\delta^{41}K_{plasma}$ = 0‰). $\delta^{41}K_{plasma}$ values that are positive (●) indicate that net K^+ transport out of the tissue/cell/fluid is enriched in ^{39}K relative to K^+ transport into the tissue/cell/fluid. $\delta^{41}K_{plasma}$ values that are indistinguishable from 0 (●) indicate that the K isotope fractionation associated with K^+ transport into and out of the cell/tissue/fluid are either 0 or equal in magnitude (and thus cancel). $\delta^{41}K_{plasma}$ values that are negative (●) indicate that net K^+ transport into the cell/tissue/fluid is enriched in ^{39}K relative to K^+ transport out of the cell/tissue/fluid. **b)** A diagram of K isotope mass balance including transport by (1) K-channels, (2) K-pumps/co-transporters, (3) through pores in tight-junctions, and (4) glomerular filtration. Equation (3) solves for the $\delta^{41}K$ value of a tissue/cell relative to blood plasma assuming steady-state K isotope mass balance with bi-directional K^+ transport by both channels and pumps/co-transporters. Variables include $f_{ch}^{out/in}$, the fraction of total K^+ transport into/out of the tissue/cell that occurs through K^+ channels, Δf_{ch}, the difference in the fraction of K transport via channels (f_{ch}^{out} - f_{ch}^{in}), ε_{ch}, K isotope fractionation associated with K channels, and $\varepsilon_{p/co}$, K isotope fractionation associated with pumps/co-transporters. K isotope fractionation associated with K^+ uptake in the gut (ε_{gut}) and K^+ loss in urine (ε_{kidney}) reflect the flux-weighted average of both paracellular and transcelluar K^+ transport. For example, K isotope fractionation in the kidney will be associated with both re-absorption and secretion of K^+ in the proximal tubule, the thick ascending limb (TAL), and cells in the collecting ducts of the kidney. **c)** Correlation between intercellular [K^+] and $\Delta\delta^{41}K_{plasma}$ values for a subset of tissues from *R. norvegicus*. Also shown are the measured activities of NaKATPase (μmol P h^{-1} g^{-1}) from (49) and values of Δf_{ch} from eqn (3).

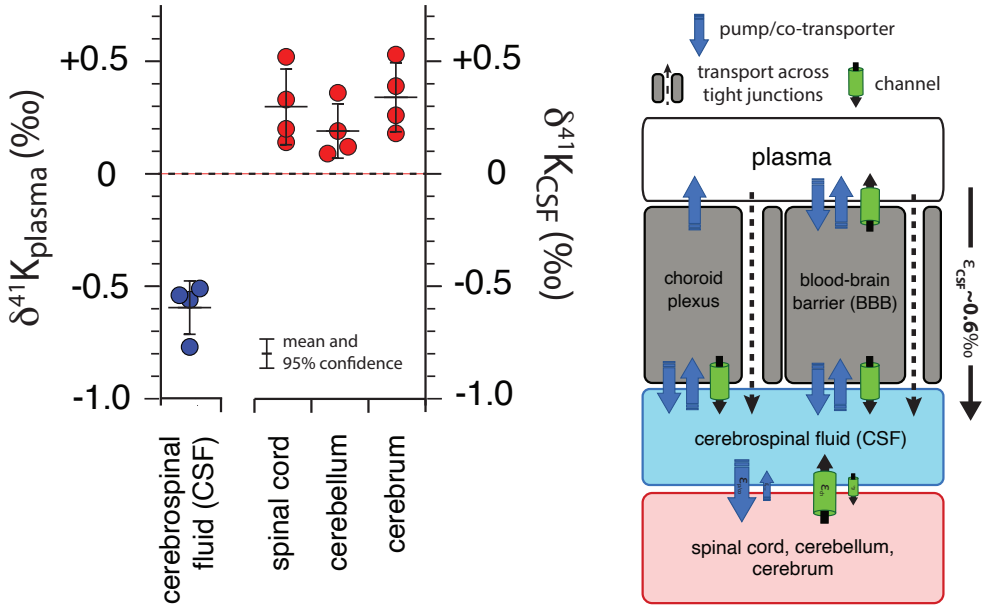

Figure 4. K isotopic composition of cerebrospinal fluid from *R. norvegicus* raised on a controlled diet normalized to blood plasma ($\delta^{41}K_{plasma}$ = 0‰) and brain tissues normalized to cerebrospinal fluid ($\delta^{41}K_{CSF}$ = 0‰) together with a diagram of K homeostasis across the choroid plexus and blood brain barrier (BBB) from (50) including transport by (1) K-channels, (2) K-pumps/co-transporters, and (3) transcellularly through pores in tight-junctions. $\delta^{41}K_{CSF}$ values that are positive (●) indicate that net K transport out of brain tissues (spinal cord, cerebellum, and cerebrum) and into CSF is enriched in ^{39}K relative to K transport from CSF into these tissues. The negative $\delta^{41}K_{plasma}$ values (●) for CSF indicate that net K transport into CSF from blood plasma is enriched in ^{39}K relative to K transport from CSF to blood plasma andreflects the flux-weighted average of the tranporters that dominate K exchange across both the choroid plexus and BBB.

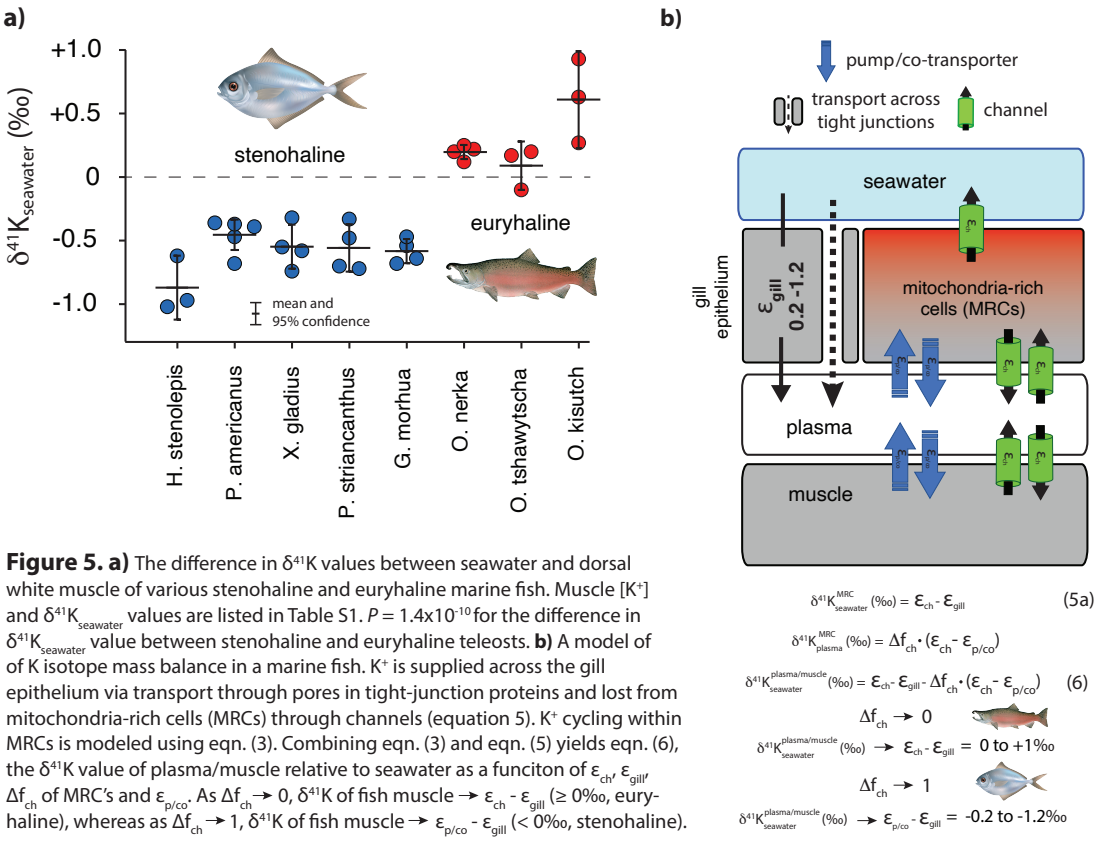

Figure 5. a) The difference in $\delta^{41}K$ values between seawater and dorsal white muscle of various stenohaline and euryhaline marine fish. Muscle $[K^+]$ and $\delta^{41}K_{seawater}$ values are listed in Table S1. $P = 1.4 \times 10^{-10}$ for the difference in $\delta^{41}K_{seawater}$ value between stenohaline and euryhaline teleosts. **b)** A model of of K isotope mass balance in a marine fish. K^+ is supplied across the gill epithelium via transport through pores in tight-junction proteins and lost from mitochondria-rich cells (MRCs) through channels (equation 5). K^+ cycling within MRCs is modeled using eqn. (3). Combining eqn. (3) and eqn. (5) yields eqn. (6), the $\delta^{41}K$ value of plasma/muscle relative to seawater as a funciton of ε_{ch}, ε_{gill}, Δf_{ch} of MRC's and $\varepsilon_{p/co}$. As $\Delta f_{ch} \rightarrow 0$, $\delta^{41}K$ of fish muscle $\rightarrow \varepsilon_{ch} - \varepsilon_{gill}$ ($\geq$ 0‰, euryhaline), whereas as $\Delta f_{ch} \rightarrow 1$, $\delta^{41}K$ of fish muscle $\rightarrow \varepsilon_{p/co} - \varepsilon_{gill}$ (< 0‰, stenohaline).